

# Cupric Oxide Nanorods on Double-Face Copper Micropuzzles Electrode as Promising Anode Materials for Lithium Ion Batteries

Huan Pang<sup>1,2,3,\*</sup>, Jiawei Deng<sup>1</sup>, Bo Yan<sup>1</sup>, Yahui Ma<sup>1</sup>, Guochang Li<sup>1</sup>, Yanning Ai<sup>1</sup>, Jing Chen<sup>1</sup>, Jiangshan Zhang<sup>1</sup>, Honghe Zheng<sup>2\*</sup> and Jimin Du<sup>1\*</sup>

<sup>1</sup> College of Chemistry and Chemical Engineering, Anyang Normal University, Anyang, 455000 Henan, P.R. China.

<sup>2</sup> School of Energy, Soochow University, Suzhou, Jiangsu, 215006, P.R. China.

<sup>3</sup> State Key Laboratory of Coordination Chemistry, Nanjing University, Nanjing, 210093 Jiangsu, P.R. China.

\*E-mail: [huanpangchem@hotmail.com](mailto:huanpangchem@hotmail.com); [hhzheng@suda.edu.cn](mailto:hhzheng@suda.edu.cn); [djm@iccas.ac.cn](mailto:djm@iccas.ac.cn)

Received: 6 August 2012 / Accepted: 30 September 2012 / Published: 1 November 2012

---

CuO nanorods on double-face Cu micropuzzles have been successfully prepared via a simple calcination approach. Electrochemical examination reveals that the CuO nanorods on double-face Cu superstructures have a reversible capacity of 645 mAh g<sup>-1</sup> and are favorable for improving the electrode kinetics. This kind of material is promising for using in lithium ion batteries.

---

**Keywords:** CuO nanorods; Cu micropuzzles; Superstructures; Lithium ion batteries;

## 1. INTRODUCTION

One dimensional (1D) nanostructures, nanowires/rods, are perfect building blocks for functional nanodevices and efficient electron and exciton transport [1-2]. Commonly, electrical conductivity is one of the most important factors affecting the utilization of active materials and the internal resistance of the electrode [3]. Therefore, synthesis of one-dimensional nanostructures of higher electrical conductivity is highly desirable in the field of nanoelectrode materials.

Recently, several techniques for the synthesis of metal oxide-metal composites become available [4-8]. The composites have a stronger ability to promote electron transfer than metal oxide because of inner electric metal, which is in the center of the composite. As the result, the composites could supply more efficient transport passage for the electrochemical processes [7-8].

As the development of nanoscience, it is reasonable to expect that the ability to process nanostructured metal oxide into nanostructured mother metal materials. This could enrich our understanding of its fundamental properties and enhance its performance in currently existing applications.

In recent years, cupric oxide (CuO) nanostructures have attracted great interest because of their fundamental importance and promising applications into electrochromic devices, optical switching, solar cells, heterogeneous catalysis, photocatalysis, gas sensing, field emission, lithium batteries and so on [9-25]. With advantages of high theoretical capacity ( $670 \text{ mAh g}^{-1}$ ), improved safety than graphite, low cost and environmental benignity, CuO is a very appealing candidate for the substitution of a conventional graphite anode in lithium ion batteries. Nanostructured CuO not only enables easy diffusion of Li ions, the strain associated with Li uptake could also be well accommodated, contributing to better electrochemical cycling performance.

Several groups have successfully synthesized CuO nanostructures onto bulk copper foil or other bulk materials [28-30], however, there is only single face of the bulk substrates to grow CuO nanostructures and assemble advanced application device. This assembly has relative lower surface area of CuO nanostructures. The novel characteristics that are always acquired from nanostructured CuO might be strongly influenced by the bulk substrates or other nonelectric substrates properties because they can grow only on the bulk substrate. Hence, to find a facile, mild way to grow CuO nanostructures on the Cu nanostructures and extend their applications are of great scientific and technological significance.

Previously, we used glucose, one of the biomolecules, to assist the synthesis of brand new puzzle-like copper superstructures and applied them to nonenzymatic glucose sensors [31]. In this work, we use these copper superstructures to calcine under different temperatures. A new structured composite, CuO nanorods on double-face Cu micropuzzles is obtained. These CuO-Cu superstructures composites can be used as lithium ion battery anode materials. The electrodes containing CuO nanorods on double-face Cu micropuzzles exhibited an electrochemical capacity of  $> 640 \text{ mA h g}^{-1}$ , and satisfactory electrochemical stability up to 300 charge–discharge cycles.

## 2. EXPERIMENTAL

### 2.1 Synthesis

**Synthesis of CuO nanorods on Cu foil substrate:** A Cu foil ( $2 \text{ cm} \times 2 \text{ cm}$ ) was calcined in the air at  $400 \text{ }^\circ\text{C}$  for 120 minutes (the product was named P1), the heating-up rate was  $1 \text{ }^\circ\text{C per min}$ .

**Synthesis of CuO nanorods on Cu superstructures:** (1) For Cu superstructures, in a typical procedure, the starting solution was prepared by mixing 0.1 g of glucose and 0.16 g of  $\text{CuSO}_4 \cdot 5\text{H}_2\text{O}$  in 10 mL of  $\text{H}_2\text{O}$ . The resulting solution was transferred into 50 mL stainless-steel autoclaves lined with poly (tetrafluoroethylene) (PTFE, Telfon). The autoclave was sealed and maintained at  $160 \text{ }^\circ\text{C}$  for 8 h and then cooled to room temperature. The red products obtained at

the bottom of the autoclave were collected, washed three times with deionized water, and dried in air; (2) For CuO nanostructures on Cu superstructures, the pure Cu superstructures were calcined in the air at 300 °C for 60 minutes (the product was named P2), P3 at 400 °C for 60 min, P4 at 400 °C for 120 min, P5 at 400 °C for 1440 min, respectively. The heating-up rate was 1 °C per min for all samples.

## 2.2 Preparation of lithium ion battery electrodes

The anode materials (based CuO mass) were fabricated by mixing P2-P5 powders, acetylene black, and PVDF at a weight ratio of 70:20:10 (P1, CuO nanorods on Cu foil was used as electrode directly), respectively, using N-methylpyrrolidone (NMP) as a solvent. The resulting slurries were cast onto copper current collectors, and then dried at 120 °C under vacuum for 12 h. The electrode foils were pressed at a pressure of  $8.27 \times 10^6$  Pa, and then cut into disks 13 mm in diameter. CR2016 coin-type cells were assembled in an argon-filled glove box (M-braun MB20G) by stacking a microporous polypropylene separator (Celgard 2400) containing a liquid electrolyte of LiClO<sub>4</sub> (1.0 M) in ethylene carbonate (EC)/dimethyl carbonate (DMC) (1:1, v/v) between the anode and the lithium metal foil.

## 2.3 Characterization

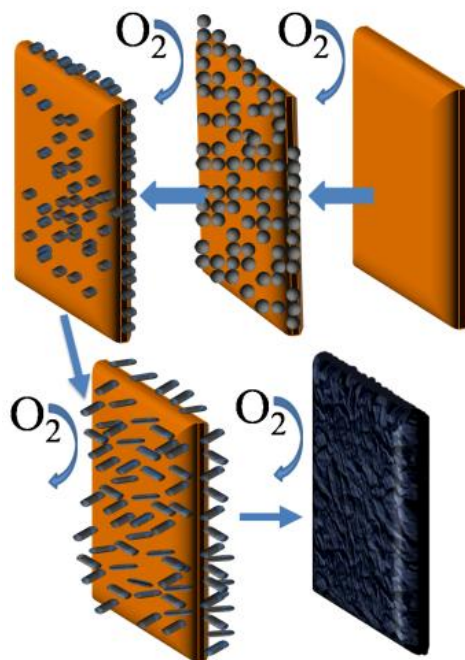
The morphology of the as-prepared samples was observed by a JEOL JSM-6701F field-emission scanning electron microscope (FE-SEM) at an acceleration voltage of 5.0 kV. The phase analyses of the samples were performed by X-ray diffraction (XRD) on a Ultima III with Cu K $\alpha$  radiation ( $\lambda = 1.5418$  Å). Transmission electron microscopy (TEM) images and HRTEM image were captured on the JEM-2100 instrument microscopy at an acceleration voltage of 200 kV.

The batteries were tested on Land CT2001A. The cyclic voltammogram (CV) were performed on an electrochemical station-CHI 660d. Electrochemical impedance spectroscopy (EIS) measurements of all the samples were conducted at open circuit voltage in the frequency range of 100 kHz to 0.01 Hz with AC voltage amplitude of 5 mV using PARSTAT2273.

## 3. RESULTS AND DISCUSSION

The CuO nanostructures on double-face Cu micropuzzles were fabricated through an easy route as shown in Scheme 1. Fig. 1 shows XRD patterns of the CuO nanostructures on Cu superstructures prepared under different conditions and CuO nanorods on Cu bulk foil. In Fig. 1, the diffraction peaks with \* marked at 43.49, 50.62 and 74.29 can be indexed to Cu (JCPDS No. 04-0836), which are generated from the Cu superstructures or Cu bulk foil. The other diffraction peaks with # marked can be indexed as CuO (JCPDS card No. 05-0661). These results suggest that CuO crystals have formed on the Cu superstructures or Cu bulk foil and the amount of CuO

increases with calcination time.



**Scheme 1.** An easy route of synthesising CuO nanostructures on double-face Cu micropuzzles.

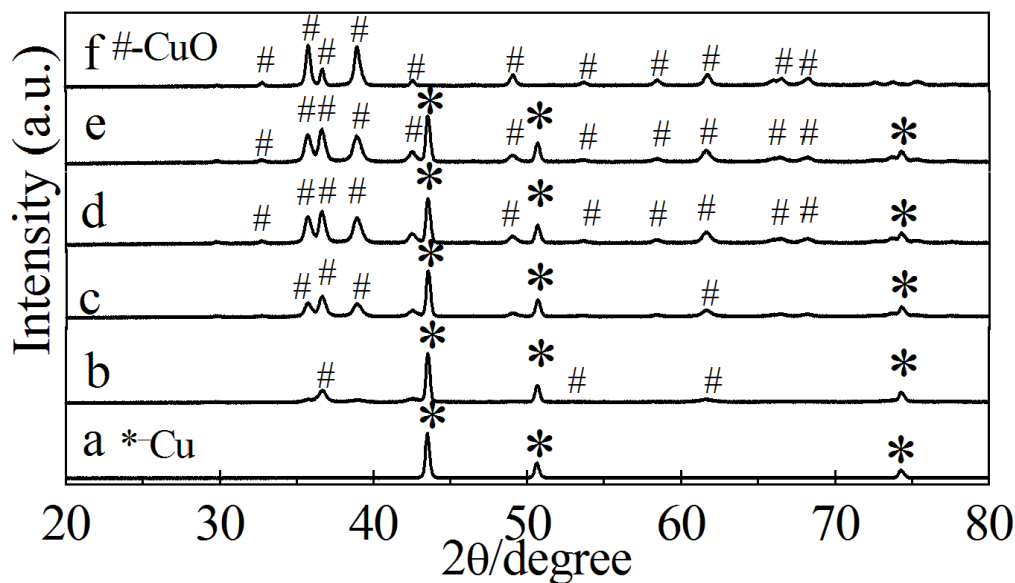


**Figure 1.** XRD patterns of (a) Cu micropuzzles and CuO nanostructures on Cu superstructures prepared under different conditions. (b) 300 °C for 60 minutes, named P2; (c) 400 °C for 60 min, named P3; (d) 400 °C for 120 min, named P4; (e) Cu foil calcined at 400 °C for 120 min, named P1; (f) 400 °C for 1440 min, named P5 respectively.

From Fig. 2a, we can see that Cu micropuzzles can be synthesized. The yield of these structures is very high, and almost all of the crystals have highly ordered structures. Fig. 2b are SEM images with higher magnifications, in which the details of the plate structure can be clearly

observed. These puzzle-like structures are formed by many polygonal mini-plates, which are not uniform in morphology; they are about several micrometres in size and assembled in two dimensions to form a large plate with size up to tens of micrometers.

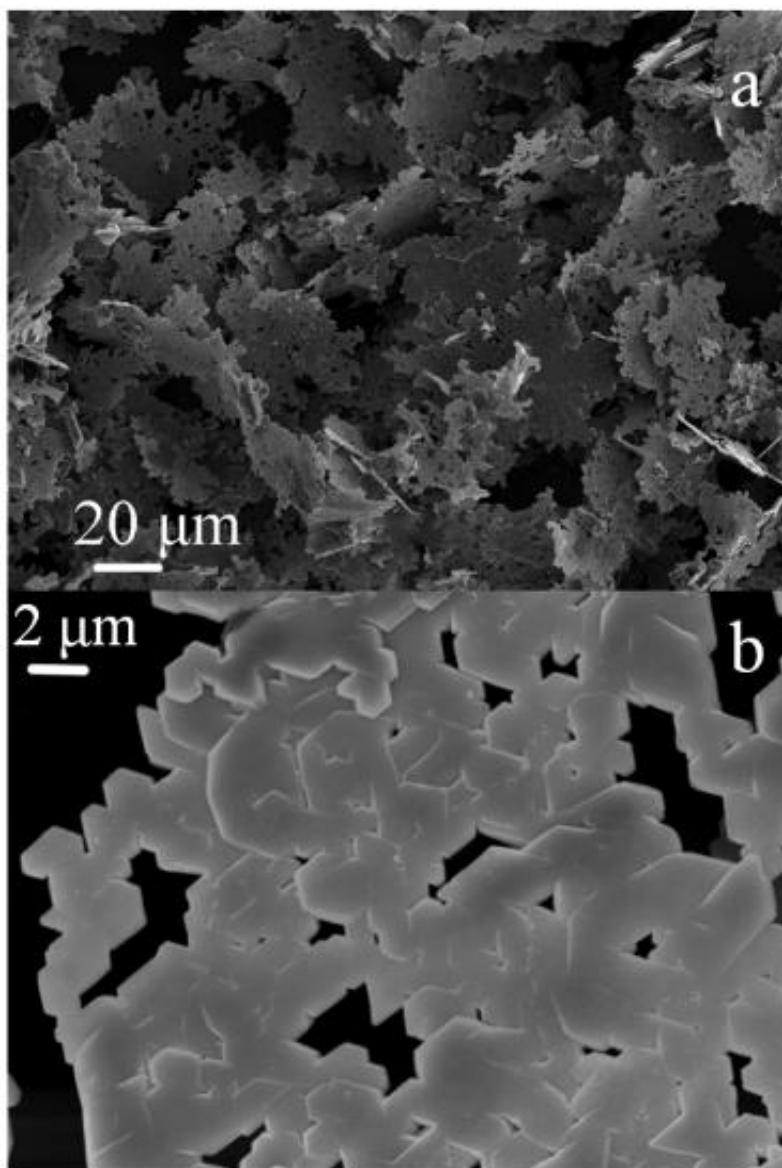


**Figure 2.** SEM images of the Cu micropuzzles at different magnifications.

Fig. 3a and b display SEM images of CuO nanostructures on the Cu superstructures prepared through calcination in the air at 300 °C for 60 minutes (P2). It is seen that only irregular seed-like particles are obtained and the surface is not smooth as the pure Cu puzzle superstructure. For the sample treated at 400 °C for 60 minutes (P3), the micropuzzle superstructure was maintained as shown in Fig. ESI 1, and there are some short nanorods on the mother Cu superstructure in Fig. 3c. The length of short nanorods is about 300-400 nm as seen in Fig. 3d. When calcined at 400 °C for 120 min (P4), a large number of epitaxial CuO nanorods are attached

to the Cu superstructure as seen in Fig. 3e-f. The length of CuO nanorods is not very uniform. The longest rod of ca. 600-700 nm, is dispersed on the double-face of the Cu superstructure as shown in Fig. 3f. When the calcination time is increased to 1440 minutes at 400 °C (P5), no nanorods can be seen on the surface of Cu superstructures. Instead, there are layers of CuO particles on the surface of superstructures, which shows an incompact structure as shown in Fig. 3h. The Cu foil calcined at 400 °C for 120 minutes (P1) has many CuO nanorods with 300-400 nm on the surface of Cu bulk foil (Fig. ESI 2).

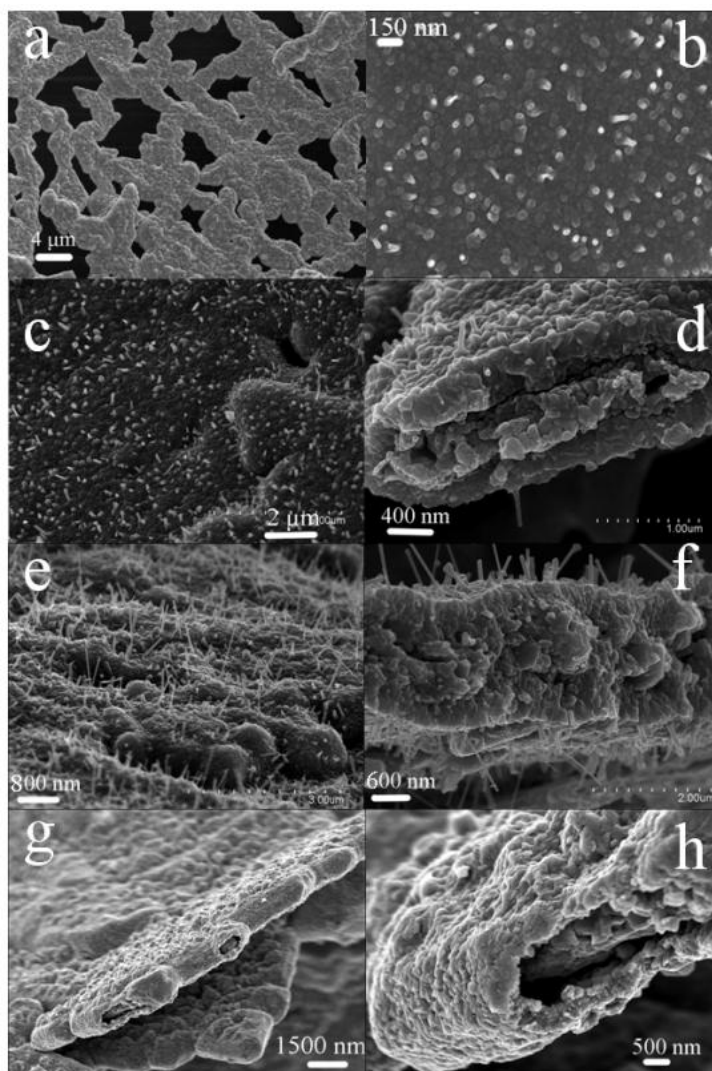


**Figure 3.** SEM images of different CuO nanostructures on the Cu superstructures prepared with calcined in the air at different calcination conditions, (a-b) 300 °C for 60 minutes, P2; (c-d) 400 °C for 60 min, P3; (e-f) 400 °C for 120 min, P4; (g-h) 400 °C for 1440 min, P5 respectively.

From Fig. 4a, we can see that the border is clear and no oxide layer can be seen. It is obvious that there are a layer of CuO nanofilm on the Cu in Fig. 4b, and the thickness is about 20-30 nm for P2. With increasing calcination time, the thickness of CuO film is increased to about

300-400 nm for P3. When calcination time was increased to 120 minutes at 400 °C for P4, CuO nanorods with 50-90 nm diameter can be seen clearly in Fig. 4d. From Fig. 4e, we found that the CuO nanorod was a single nanocrystal with (111) crystal plane. And the single nanocrystal CuO nanorod might promote electron transfer during charge-discharge processing.

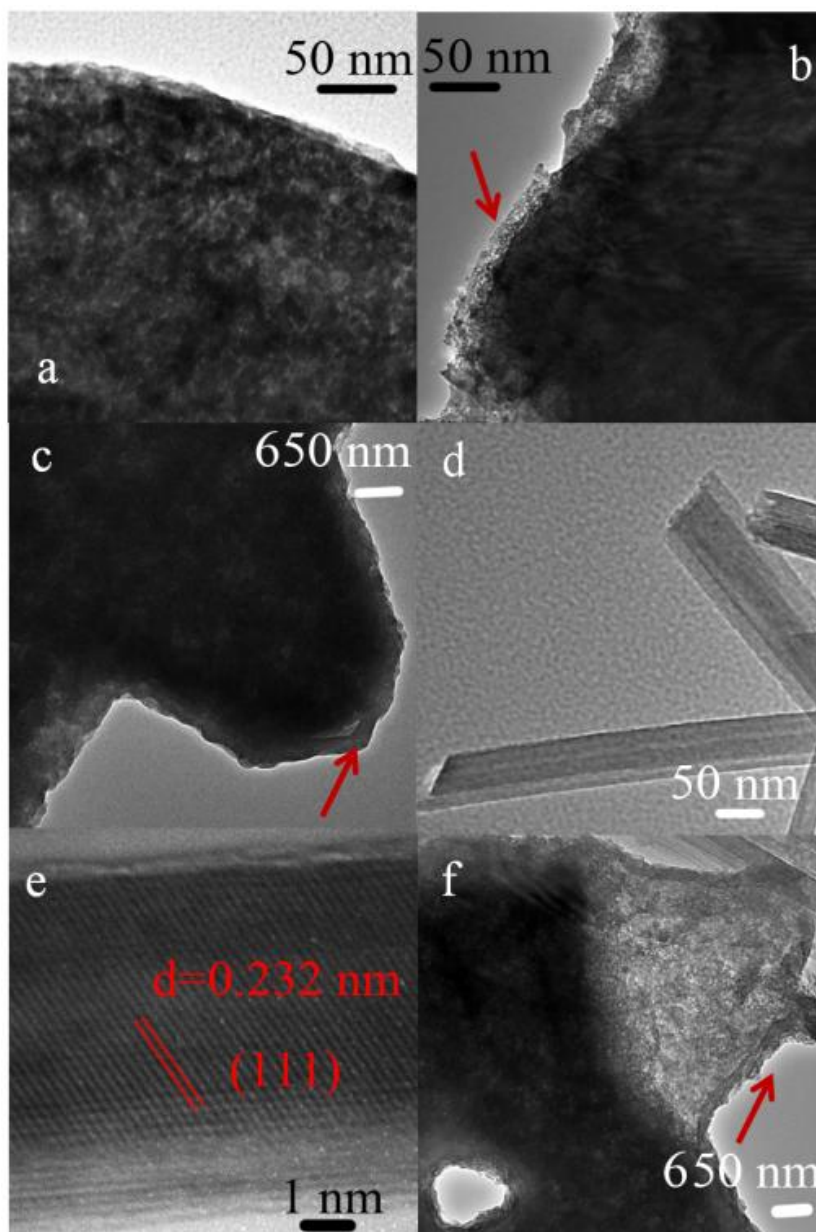


**Figure 4.** TEM images (a) Cu Cu puzzle superstructure; (b) P2; (c) P3; (d-e) P4; (f) P5

When we have increased calcination time to 1440 minutes at 400 °C (P5), there are layers of CuO particles on the surface of superstructures, which showed an incompact structure as SEM images shown in Fig. 3h.

Brunauer-Emmett-Teller (BET) determination was performed to examine the specific structural properties of these samples. The BET surface areas for P2-P5 samples are 8.6, 8.3, 10.5,

11.2 and  $16.2 \text{ m}^2 \text{ g}^{-1}$  respectively. Though P2-P5 do not have large BET surface areas, we can see that P5 have the largest one which make the efficient contact of the electrolyte with CuO-Cu composite materials.

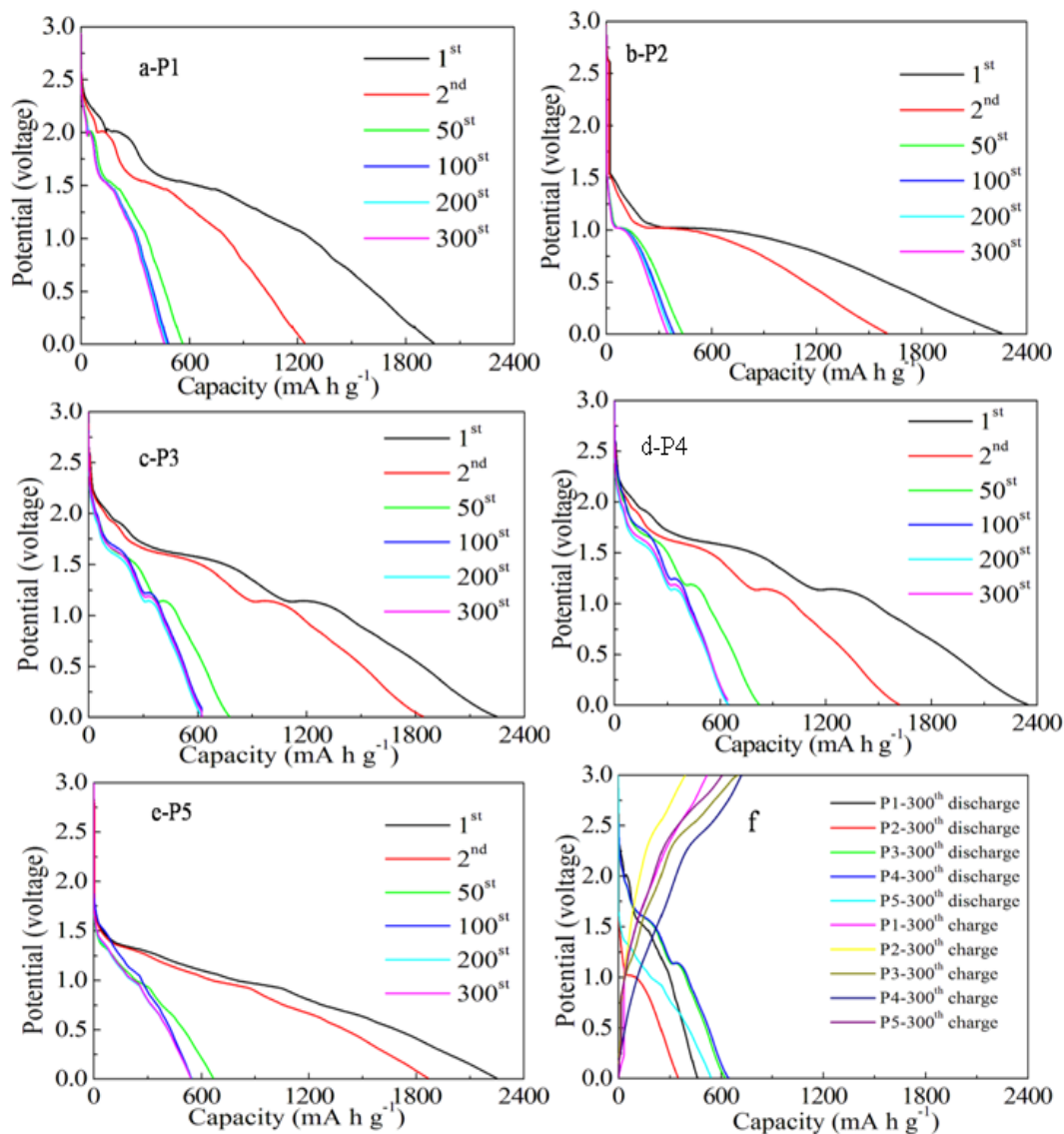


**Figure 5.** (a-e) Discharge curves of the cells made from the as-prepared P1-P5 materials between 0.01–3.0 V at 0.5 C and room temperature, the numbers indicate the corresponding cycle number; (f) Charge-discharge curves at 300<sup>th</sup> cycle.

Simply by controlling the calcination condition, different CuO nanocomposite superstructures including P2-P5 have been obtained. Fig. 5a-e show discharge curves of the cells made from the as-prepared P1-P5 materials between 0.01–3.0 V at 0.5 C and room temperature, the numbers indicate the corresponding cycle number. As can be seen from Fig. 5, the first cycle discharge capacities for the as-synthesized P1-P5 electrodes were 1957, 2258, 2247, 2345 and 2249 mA h g<sup>-1</sup>, respectively. Correspondingly, the first charge capacities were obtained to be 1861,

2158, 2130, 2141 and 2139 mAh g<sup>-1</sup>. The irreversible capacity loss of 60 % in the first cycle is believed to be mainly ascribed to diverse irreversible processes such as interfacial lithium storage, inevitable formation of solid electrolyte interface (SEI layer) and organic conductive polymer, as well as the electrolyte decomposition. These irreversible reactions are very typical for most anode materials in lithium ion cells [32-36]. All the electrodes show a certain capacity fade upon prolonged cycling. However, P4 composite electrodes maintained fairly high Li-ion insertion/deinsertion capacity even after 300 cycles. Compared with the other P1-P3 and P5 electrodes. In Fig. 5f, we can see that P4 have good cycling performance which retain >640 mAh g<sup>-1</sup> after 300 cycle.

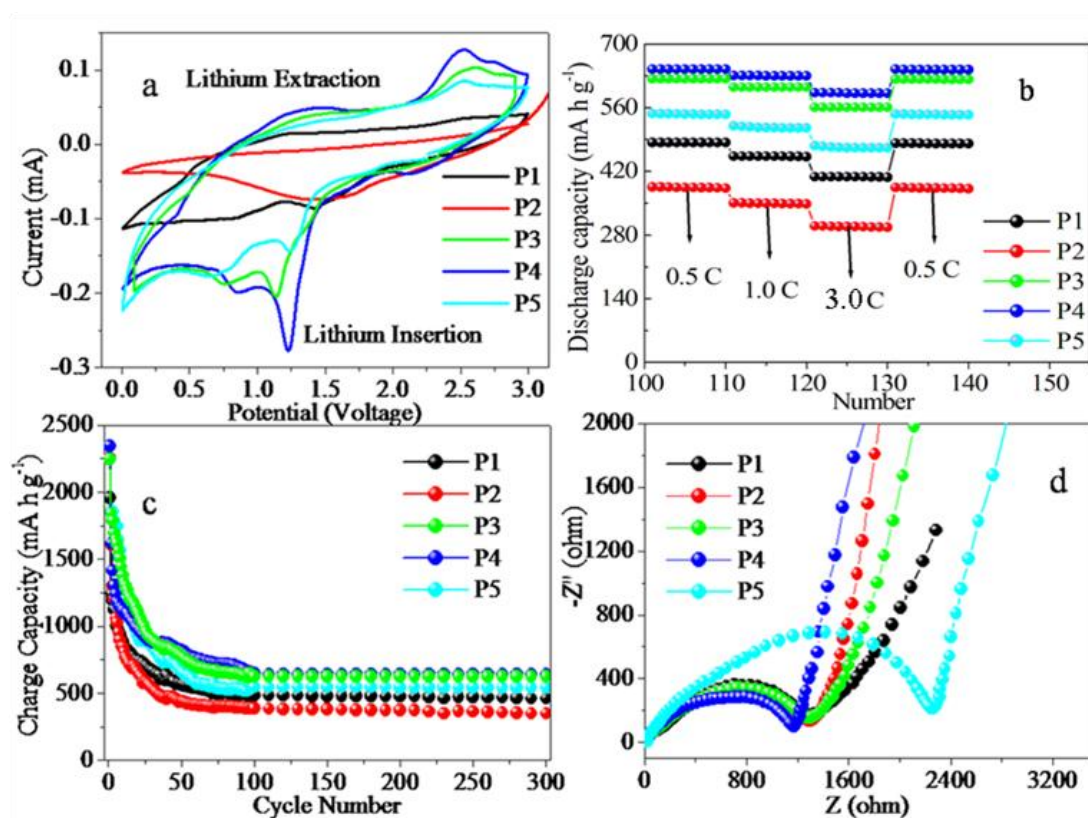


**Figure 6.** (a) Cyclic voltammograms of the electrode; (b) the cycling performance of the electrodes at 0.5-3.0 C; (c) the long cyclic performances of the electrodes at 0.5 C; (d) the electrochemical impedance spectra (EIS) of the electrodes at room temperature.

As the structure and electrochemical properties of the electrochemically activated material are always influenced by the original structure of the as-prepared electrodes, P1-P5 composites were subjected to long-term cycling test (300 cycles). Cycling performances are important in gaining further understanding on the lithium insertion-extraction mechanism of composites electrodes. Fig. 6a shows cyclic voltammograms of the electrode (P1-P5) with a scan rate of 0.1 mV s<sup>-1</sup> after 300 charge-discharge cycles. It is clear there are two reduction peaks in the potential range of 0.65–1.25 V for P3, P4 and P5, while no distinct reduction peak is observed for P1, P2.

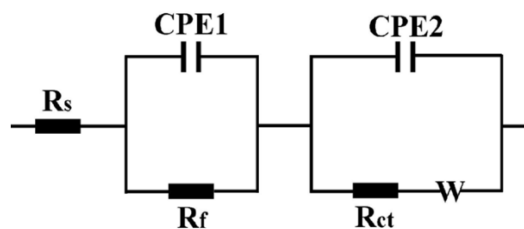
The reduction peaks correspond to a multi-step electrochemical reaction which involves (i) the creation of a  $\text{Cu}^{\text{II}}_{1-x}\text{Cu}^{\text{I}}_x\text{O}_{1-x/2}$  solid solution with CuO phase, (ii) the formation of  $\text{Cu}_2\text{O}$  phase, and (iii) the decomposition of  $\text{Cu}_2\text{O}$  into Cu and  $\text{Li}_2\text{O}$  [37]. This is consistent with discharge-charge curves with a multiple-plateau feature as shown in Fig. 5f. The strong reduction peak at 1.2 V and the corresponding oxidation peak at 2.5 V demonstrate the excellent charge-discharge stability of P4.

Fig. 6b displays the rate performance of P1-P5 at 0.5-3.0 C. The specific capacities for P1-P5 at 0.5 C (1 C=670 mA  $\text{g}^{-1}$ ) were obtained to be 483, 383, 545, 645 and 624 mAh  $\text{g}^{-1}$ , respectively. At 3.0 C, all the electrodes still retained most of their capacity at 0.5C, specifically, 406 (84.0% of 0.5 C), 297 (77.5% of 0.5 C), 471 (86.4% of 0.5 C), 592 (91.8% of 0.5 C), and 561 mAh  $\text{g}^{-1}$  (89.9% of 0.5 C) were obtained for P1-P5, respectively. This shows that the electrodes are capable of good rate performance.

Long-term cycling performances for P1-P5 electrodes at 0.5 C are illustrated in Fig. 6c. By comparison, P4 exhibits relatively low capacity decay and retain a high capacity of 645 mAh  $\text{g}^{-1}$  after 300 cycles. Apparently, the formation of CuO nanorods on the double-face of Cu micropuzzle composite is crucial to the improvement of electrochemical performance of the integrated CuO-Cu electrodes. The loose texture and sufficient space between the nanorods allow fast lithium ion flux across the interface and better accommodate the volume change induced by lithium insertion/extraction, as well as preventing the nanoparticles from agglomeration. More importantly, the one dimensional CuO nanorods not only contributes to the improved electrode stability because of the reduced lattice strain associated with lithium intercalation, but also increases the efficiency for charge transport because of the short diffusion length [38]. In addition, Cu micropuzzle is in the center of the composite, typically several micrometers, need only a few contact points with the current collector to ensure electron transport, which improves the lithium-ion intercalation, whereas single CuO nanoparticle counterparts may easily become electrically isolated as they expand or contract during battery reactions [39]. These features may also favor the improvement of the cycling stability of the present CuO-Cu composite electrodes.

To understand the electrode kinetics, the as-prepared P1-P5 for lithium intercalation were estimated by electrochemical impedance spectra (EIS). Fig. 6d shows the EIS of the electrodes of P1-P5 at room temperature. In general, the impedance curves present two partially overlapped semicircles in the high- and medium-frequency regions and an inclined line in the low-frequency region. An equivalent circuit used to fit the impedance curve is given in Fig. 7. This is similar to the circuit employed for the anode of the lithium ion battery. The semicircle can be assigned to the combination of the electrode-electrolyte interface film resistance ( $R_f$ ) and the charge transfer impedance ( $R_{ct}$ ), while the linear portion is designated to Warburg impedance ( $W$ ), which is attributed to the diffusion of lithium ions into the bulk of the electrode materials. The charge-transfer resistance  $R_{ct}$  was calculated by ZSimWin software to be 20.6, 17.3, 12.9, 10.4 and 26.4  $\Omega$ , respectively. The CuO nanorod-Cu composites have a stronger ability to promote electron transfer than CuO oxide nanoparticle-Cu because of the one dimensional nanostructure property [1, 2, 40, 41] and inner electric Cu metal which is in the center of the composite. In addition, the charge-transfer resistance  $R_{ct}$ , also called Faraday resistance, is a limiting factor for the specific power of

battery. It is the low Faraday resistance that results in the high specific power of the P4 composite electrode.



**Figure 7.** The equivalent circuit for the electrochemical impedance spectrum. It consists of the electrolyte ( $R_s$ ), surface film ( $R_f$ ) and charge transfer ( $R_{ct}$ ) resistances, constant phase elements (CPE1 and CPE2), along with the Warburg impedance ( $W$ ).

#### 4. CONCLUSIONS

In summary, CuO nanorods on double-face Cu superstructures have been successfully prepared via a simple calcination approach. The morphologies and sizes of the as-prepared CuO-Cu composites were well controlled by varying the reaction parameters. The CuO nanorods on double-face Cu superstructures (P4) are favorable for increasing the discharge capacity and improving the electrode kinetics. P4 exhibited a high discharge capacity of  $645 \text{ mAh g}^{-1}$  (at 0.5 C) after 300 cycles. The present results suggests that CuO nanorods on double-face Cu superstructures are promising anode materials in lithium ion batteries.

#### ACKNOWLEDGEMENTS

This work is supported by the National Natural Science Foundation of China (21201010, 21073129, 21071006), the Department of Science and technology of China for the 863 project (2009AA03Z225863). Henan Province of Science & Technology Foundation (122102210253) and the project of Science & Technology of Anyang city.

*Electronic Supplementary Information (ESI) available: [SEM images of P1 and P4].*

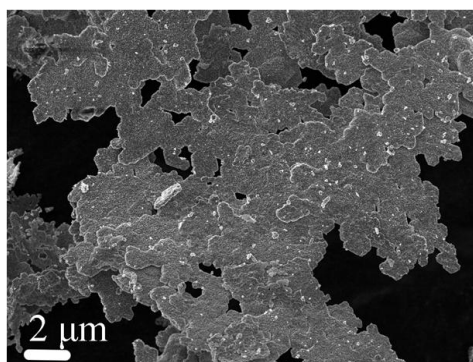


**Figure ESI 1.** SEM image of CuO nanorods on Cu superstructures-P4, 400 °C for 60 minutes.

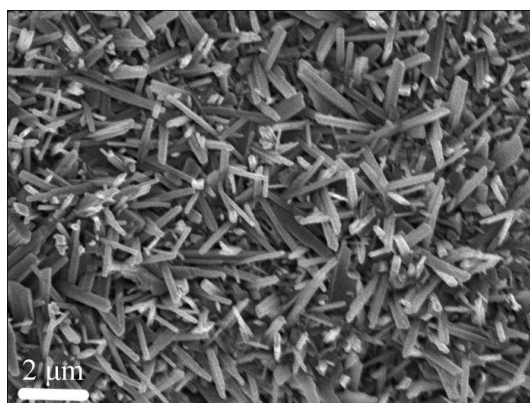


**Figure ESI 2.** SEM image of CuO nanorod on the Cu bulk foil.

## References

1. C. Z. Wu, J. Dai, X. D. Zhang, J. L. Yang and Y. Xie, *J. Am. Chem. Soc.* 131 (2009) 7218.
2. Y. Huang, X. F. Duan, Y. Cui, L. J. Lauhon, K. H. Kim and C. M. Lieber, *Science* 294 (2001) 1313.
3. M. S. Wu and H. H. Hsieh, *Electrochimica. Acta.* 53 (2008) 3427.
4. Tracy, J. B.; Weiss, D. N.; Dinega, D. P. and Bawendi, M. G. *Phys. Rev. B* 72 (2005) 064404.
5. Tracy, J. B.; Bawendi and M. G. *Phys. Rev. B* 74 (2006) 184434.
6. A. C. Johnston-Peck, J. W. Wang and J. B. Tracy, *ACS Nano* 4 (2010) 1913–1920.
7. X. J. Zhang, G. F. Wang, W. Zhang, N. J. Hu, H. Q. Wu and B. Fang, *J. Phys. Chem. C* 112 (2008) 8856-8862.
8. E. Hosono, S. Fujihara, I. Honma and H. S. Zhou, *Electrochem. Commun.* 8 (2006) 284-288.
9. T. J. Richardson, J. L. Slack and M.D, *Electrochim. Acta* 46 (2001) 2281.
10. D. V. Morgan and M. J. Howes, *Phys. Status Solidi A* 21 (1974) 191.
11. R. P. Wijesundera, *Semicond. Sci. Technol.* 25 (2010) 045015.
12. S. Anandan, X. Wen and S. Yang, *Mater. Chem. Phys.* 93 (2005) 35.
13. M. Zhou, Y. Gao, B. Wang, Z. Rozynek and J. O. Fossum, *Eur. J. Inorg. Chem.* (2010) 729.
14. K. E. Toghill and R. G. Compton, *Int. J. Electrochem. Sci.* 5 (2010) 1246.
15. S. P. Chang and T. H. Yang, *Int. J. Electrochem. Sci.* 7 (2012) 5020.
16. P. Wang, Y. N. N. Li, J. Yang and Y. Zheng, *Int. J. Electrochem. Sci.* 1 (2006) 122-129.
17. X. H. Huang, J. B. Wu, Y. Lin, R. Q. Guo, *Int. J. Electrochem. Sci.* 7 (2012) 6611-6621
18. Z. Ai, L. Zhang, S. Lee and W. Ho, *J. Phys. Chem. C* 113 (2009) 20896.
19. M. Vaseem, A. Umar, Y. B. Hahn, D. H. Kim, K. S. Lee and J. S. Jang, *Catal. Commun.* 10 (2008) 11.
20. M. Paschoalino, N. C. Guedes, W. Jardim, E. Mielczarski, J. A. Mielczarski, P. Bowen and J. Kiwi, *J. Photochem. Photobiol A* 199 (2008) 105.
21. A. Chowdhuri, P. Sharma, V. Gupta, K. Sreenivas and K. V. Rao, *J. Appl. Phys.* 92 (2002) 2172.
22. Y. W. Zhu, T. Yu, F. C. Cheong, X. J. Xu, C. T. Lim, V. B. C. Tan, J. T. L. Thong and C. H. Sow, *Nanotechnology* 16 (2005) 88.
23. Y. Liu, L. Zhong, Z. Peng, Y. Song and W. Chen, *J. Mater. Sci.* 45 (2010) 3791.
24. J. Y. Xiang, J. P. Tu, L. Zhang, Y. Zhou, X. L. Wang and S. J. Shi, *J. Power Sources* 195 (2010) 313.
25. A. Comanac, L. De Medici, M. Capone and A. J. Millis, *Nat. Phys.* 4 (2008) 287.
26. Z. Wang, F. Su, S. Madhavi. and X. W. Lou, *Nanoscale* 3 (2011) 1618-1623.
27. J. C. Park, J. Kim, H. Kwon and H. Song, *Adv. Mater.* 21 (2009) 803–807.
28. X. Jiang, T. Herricks and Xia, Y. *Nano Lett.* 2 (2002) 1333.

29. X. Wen, Y. Xie, C. L. Choi, K. C. Wan and X. Y. Li and S. Yang, *Langmuir* 21 (2005) 4729.
30. A. U. Akrajas and O. Munetaka, *Cryst. Growth Des.* 12 (2007) 2404.
31. H. Pang, Q. Y. Lu, J. J. Wang, Y. C. Li and F. Gao, *Chem. Commun.* 46 (2010) 2010.
32. J. Maier, *Nat. Mater.* 4 (2005) 805.
33. X. W. Lou, C. M. Li and L. A. Archer, *Adv. Mater.* 21 (2009) 2536.
34. X. W. Lou, D. Deng, J. Y. Lee, J. Feng and L. A. Archer, *Adv. Mater.* 20 (2008) 258.
35. S. Laruelle, S. Grugeon, P. Poizot, M. Dolle, L. Dupont and J. M. Tarascon, *J. Electrochem. Soc.* 149 (2002) A627.
36. Z. Y. Wang, F. B. Su, S. Madhavi and X. W. Lou, *Nanoscale* 3 (2011) 1618–1623.
37. A. Debart, L. Dupont, P. Poizot, J. B. Leriche and J. M. Tarascon, *J. Electrochem. Soc.* 148 (2001) A1266.
38. H. J. Fan, P. Werner and M. Zacharias, *Small* 2 (2006) 700.
39. P. G. Bruce, B. Scrosati and J. M. Tarascon, *Angew. Chem. Int. Ed.* 47 (2008) 2930.
40. H. Pang, Q. Y. Lu, Y. C. Li and F. Gao, *Chem. Commun.* (2009) 7542.
41. X. Wang, D. M. Tang, H. Q. Li, W. Yi, T. Y. Zhai, Y. Bando and D. Golberg, *Chem. Commun.* 48 (2012) 4812-4814.